OPEN ACCESS Freely available online

PLOS ONE

Modeling the Electric Potential across Neuronal Membranes: The Effect of Fixed Charges on Spinal Ganglion Neurons and Neuroblastoma Cells

Thiago M. Pinto[1,2]*, Roseli S. Wedemann[1], Célia M. Cortez[1]

1 Instituto de Matemática e Estatística, Universidade do Estado do Rio de Janeiro, Rio de Janeiro, Brazil, **2** Departamento de Física, Faculdade de Filosofia, Ciências e Letras de Ribeirão Preto, Universidade de São Paulo, Ribeirão Preto, São Paulo, Brazil

Abstract

We present a model for the electric potential profile across the membranes of neuronal cells. We considered the resting and action potential states, and analyzed the influence of fixed charges of the membrane on its electric potential, based on experimental values of membrane properties of the spinal ganglion neuron and the neuroblastoma cell. The spinal ganglion neuron represents a healthy neuron, and the neuroblastoma cell, which is tumorous, represents a pathological neuron. We numerically solved the non-linear Poisson-Boltzmann equation for the regions of the membrane model we have adopted, by considering the densities of charges dissolved in an electrolytic solution and fixed on both glycocalyx and cytoplasmic proteins. Our model predicts that there is a difference in the behavior of the electric potential profiles of the two types of cells, in response to changes in charge concentrations in the membrane. Our results also describe an insensitivity of the neuroblastoma cell membrane, as observed in some biological experiments. This electrical property may be responsible for the low pharmacological response of the neuroblastoma to certain chemotherapeutic treatments.

Citation: Pinto TM, Wedemann RS, Cortez CM (2014) Modeling the Electric Potential across Neuronal Membranes: The Effect of Fixed Charges on Spinal Ganglion Neurons and Neuroblastoma Cells. PLoS ONE 9(5): e96194. doi:10.1371/journal.pone.0096194

Editor: David J. Schulz, University of Missouri, United States of America

Received January 2, 2014; **Accepted** April 4, 2014; **Published** May 6, 2014

Funding: The authors acknowledge support from the Brazilian National Council for Scientific and Technological Development (CNPq), the Rio de Janeiro State Research Foundation (FAPERJ), the São Paulo Research Foundation (FAPESP), and the Brazilian agency which funds graduate studies (CAPES). The funders had no role in study design, data collection and analysis, decision to publish, or preparation of the manuscript.

Competing Interests: The authors have declared that no competing interests exist.

* E-mail: thiagomatos@ime.uerj.br

Introduction

Electrostatic forces affect the passive and active transport of charged particles through biological membranes. The flow rate of ions through the membrane depends on the strength of the intramembranous electric field. These forces also affect the robustness of some ligands of the membrane [1]. In this work, we study the influence of surface electric charges on the stability of the cell membrane in the condition of equilibrium, by modeling the electric potential profile. The profile describes the behavior of the potential along the axis perpendicular to the cell membrane, from the outer bulk region to the inner cytoplasmic region [2–5]. We do not consider here dynamical phenomena in the structure of the membrane, and treat only the electrostatic situation, which occurs once the system has reached equilibrium. We refer the reader to studies such as [6,7] that treat dynamical, nonequilibrium phenomena, like the molecular dynamics of ion channels associated with transmembrane ion transport, using the Poisson-Nersnt-Planck theory [6] and the Poisson-Boltzmann-Nernst-Planck model [7].

The electric potential on a cell surface is determined as the difference of potential between the membrane-solution interface and the bulk region [1]. It has been shown that the electrophoretic behavior of neuroblastoma cells provides information about their surface charges, in different phases of the cellular cycle [8–10]. These experiments show that membrane anionic groups are mainly responsible for the surface charges of murine neuroblastoma cells [10]. It is known that neuroblastoma cells, like all other cancerous cells, multiply quickly. Alterations of the dynamics of cellular multiplication compromise the synthesis and structure of components of the membrane, with possible degradation of these components, promoting deformations of the structure and composition of the plasma membrane [11].

We show a detailed and revised description of the model more briefly presented by Cortez and collaborators in [3–5], which was originally used to simulate the squid giant axon. This model is based on the statistical mechanical theory of electrolyte solutions and electric double layers [12–15]. We then present a study that applies this model in a novel way to the neurons of mammals (mice) [16,17], in order to investigate the alterations of the electric potential and therefore, the capability of transmitting electric signals in the membrane of cancerous neurons. Here, the spinal ganglion neuron denotes a healthy neuron, and the neuroblastoma cell represents a tumorous neuron. With simulations of this model, we compare the effects of charges fixed onto the inner surface of the membrane and those associated with cytoplasmic proteins, on the electric potential on the surfaces of the membranes of both types of cells, considering both natural states of neurons, the resting and the action potential (AP) states. The AP state refers to the state of the neuron in which it has been stimulated enough, so that its physico-chemical conditions are such that the transmembrane potential reaches the maximum value of the AP. The temporal evolution of the transmembrane potential was not

considered. We also calculated the potential profile across the membrane, including data from electrophoretic experiments in our model.

Methods

Cortez and collaborators have proposed in [4] an axon membrane model, to study how charges fixed onto the inner surface of the membrane and those associated with cytoplasmic proteins influence the electric potential of the squid axon membrane. In their work, the effects of divalent ions were included, with a numerical solution of the model equations. In the present study, we apply this model to healthy and cancerous *mammalian* neurons, to understand electrical characteristics of the membranes of these cells. We present the formal derivation of the complete model here, since it was not shown in [3,4] and because we have found mistakes in some of the equations presented in [4]. We also describe, in Section *Surface Potentials*, a method for calculating electric potentials on the interfaces of the neuronal membrane, which was not discussed in previous work. We thus present here a more detailed and revised description of the theory and mathematical model of the electric potential across neuronal membranes in equilibrium, which was originally discussed in [4].

In the neuronal membrane model we have adopted, shown in Fig. (1), four different regions are presented: extracellular, glycocalyx, bilayer and cytoplasm. The bilayer thickness is h and the width of the glycocalyx is h_g. Surface potentials are represented as $\phi_{S_{eg}}$ for the potential on the surface S_{eg}, between the extracellular and glycocalyx regions, $\phi_{S_{gb}}$ is the potential on the surface S_{gb}, between the glycocalyx and the bilayer, and $\phi_{S_{bc}}$ is the potential on the surface S_{bc}, between the bilayer and cytoplasm. We denote by $\phi_{-\infty}$ and $\phi_{+\infty}$ the potentials at $-\infty$, in the electrolytic extracellular phase, and at $+\infty$, in the bulk cytoplasmic region, respectively.

The Electric Potential in the Membrane Regions

To determine the potential profile across the membrane, we first consider the Poisson equation [3,4,15],

$$\nabla^2\phi_i(x,y,z)=\frac{-4\pi\rho_i(z)}{\epsilon_i}, \quad \text{for } i\in\{ext,g,b,c\}, \tag{1}$$

where $\phi_i(x,y,z)$ is the electric potential in any region i; $i=ext$ for the outer electrolytic region; $i=g$ for the glycocalyx; $i=b$ for the bilayer; and $i=c$ for the cytoplasm. The volumetric charge density due to the electrolytes in solution of area i is $\rho_i(z)$, and ϵ_i is the dielectric constant in region i. There is no charge in the bilayer ($i=b$), due to its hydrophobic property, and thus $\rho_b(z)=0$.

We consider the further boundary conditions to calculate the constants of integration:

1. When z tends to an extreme value, $z\to-\infty$ (in region ext) or $z\to+\infty$ (in the cytoplasm), the electric potential tends to limiting values represented by $\phi_{-\infty}$ and $\phi_{+\infty}$, respectively. Ionic concentrations assume limiting values in the bulk regions, $\lim_{z\to-\infty}\eta_{\gamma,ext}(z)=\eta_{\gamma,-\infty}$ and $\lim_{z\to+\infty}\eta_{\gamma,e}(z)=\eta_{\gamma,+\infty}$, respectively, where γ represents an ion, such as Na^+, K^+, or Cl^-.
2. When $z=-h_g-h/2$ and $z=\pm h/2$, we consider the continuity of the electric potentials, $\phi_{S_{eg}}$, $\phi_{S_{gb}}$ and $\phi_{S_{bc}}$, respectively.
3. There is a discontinuity of the electric field vector on the surfaces between regions.

The Effect of Fixed Charges. When we include the effect of fixed charges in the model, Poisson Eq. (1) becomes

$$\nabla^2\phi_i(x,y,z)=\frac{-4\pi(\rho_i(z)+\rho_{fi})}{\epsilon_i}, \tag{2}$$

where ρ_{fi} is the density of charges fixed onto proteins of area i ($\rho_{fext}=0$, for the outer electrolytic region, ρ_{fg} for the glycocalyx, and ρ_{fc} for the cytoplasm).

The volumetric charge density $\rho_i(z)$ is the sum of the charge densities of positive and negative ions in the solution [3]

$$\rho_i(z)=\sum_{\gamma^+}eV_{\gamma^+}\eta_{\gamma^+,i}(z)+\sum_{\gamma^-}eV_{\gamma^-}\eta_{\gamma^-,i}(z), \tag{3}$$

where γ^+ represents a positive ion, and γ^-, a negative ion. The molar density for an ion γ (ionic concentration) in region i is $\eta_{\gamma,i}(z)$, and V_γ is the valency of ion γ. For example, $V_{Ca^{2+}}=2$ and $V_{Cl^-}=-1$. The absolute value of the electron charge is e. Due to the electroneutrality condition, we can write

$$\int\rho_i(z)dz=0,$$

within the boundaries of each region.

In our model, we suppose that the surfaces are infinite in the x and y directions, perpendicular to z, and that the distribution of charges in these directions is homogeneous. Considering this, and substituting Eq. (3) in Eq. (2), we obtain

$$\frac{d^2\phi_i(z)}{dz^2}=-\frac{4\pi}{\epsilon_i}\left(\sum_{\gamma^+}eV_{\gamma^+}\eta_{\gamma^+,i}(z)+\sum_{\gamma^-}eV_{\gamma^-}\eta_{\gamma^-,i}(z)\right)+a_i, \tag{4}$$

where

$$a_i=-\frac{4\pi\rho_{fi}}{\epsilon_i}. \tag{5}$$

To determine $\eta_{\gamma,i}(z)$, we use the equation for the electrochemical potential, due to an ionic solute in a diluted solution [3,4]

$$\mu_{\gamma,i}(z)=\mu^0_{\gamma,i}(P,T)+KTln(\eta_{\gamma,i}(z))+eV_\gamma\phi_i(z), \tag{6}$$

where K is Boltzmann's constant, T is the temperature, $\mu^0_{\gamma,i}(P,T)$ is the standard chemical potential, dependent on pressure and temperature, $KTln(\eta_{\gamma,i}(z))$ is a term that expresses the influence of the ionic concentration $\eta_{\gamma,i}(z)$, and $eV_\gamma\phi_i(z)$ is the contribution of the electric potential.

Applying the $\vec{\nabla}$ operator in Eq. (6) and again considering the homogeneous distribution of charges in the directions perpendicular to z, we verify that

$$\frac{d\mu_{\gamma,i}(z)}{dz}=\frac{d\mu^0_{\gamma,i}(P,T)}{dz}+KT\frac{d}{dz}ln(\eta_{\gamma,i}(z))+eV_\gamma\frac{d\phi_i(z)}{dz}. \tag{7}$$

Considering that there is a condition of Boltzmann equilibrium in the aqueous environments adjacent to the bilayer, $\frac{d\mu_{\gamma,i}(z)}{dz}=0$ and $\frac{d\mu^0_{\gamma,i}(P,T)}{dz}=0$, and Eq. (7) becomes

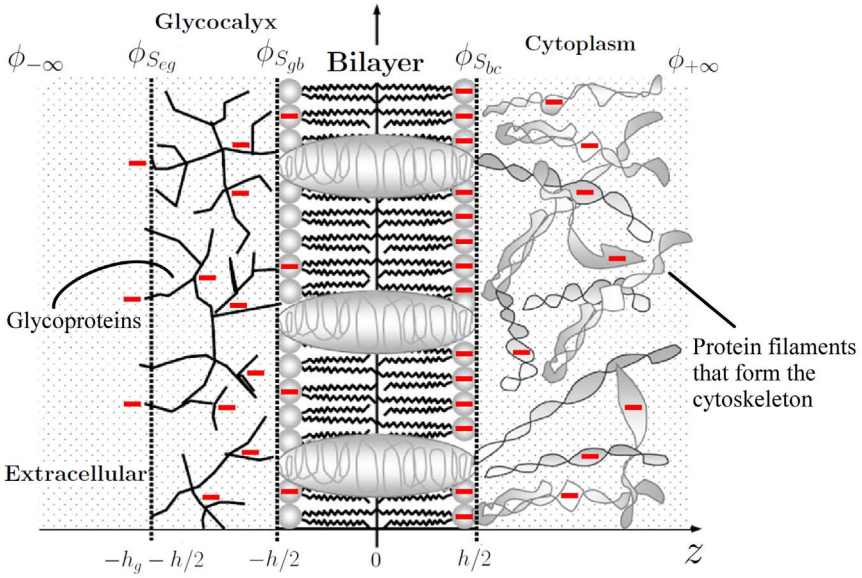

Figure 1. Model for a neuronal membrane. Different regions are presented, with the corresponding symbols for the potentials on the surfaces dividing regions. Symbols are explained in the text. Minus signs illustrate negative fixed charges on proteins.
doi:10.1371/journal.pone.0096194.g001

$$0 = KT\frac{d}{dz}ln(\eta_{\gamma,i}(z)) + eV_\gamma\frac{d\phi_i(z)}{dz}. \quad (8)$$

The integration of Eq. (8) from z in one of the three regions, extracellular, glycocalyx and cytoplasm, to a limiting boundary region, for which we have experimentally measured quantities, considering the electrolytes distributed over the adjacency of the bilayer gives

$$\int_{\eta_{\gamma,i}(z)}^{\eta_{\gamma,i,l}} KT\frac{d}{d\eta_{\gamma,i}}ln(\eta_{\gamma,i}(z))d\eta_{\gamma,i} = -\int_{\phi_i(z)}^{\phi_{i,l}} eV_\gamma\frac{d\phi_i(z)}{d\phi_i}d\phi_i, \quad (9)$$

where $\phi_{i,l}$ and $\eta_{\gamma,i,l}$ are limiting values of the electric potential and the ionic concentration of γ, respectively, in region i. The solution of Eq. (9) results in

$$\eta_{\gamma,i}(z) = \eta_{\gamma,i,l}\exp^{\left(\frac{-eV_\gamma\Delta\phi_i(z)}{KT}\right)}, \quad (10)$$

where

$$\Delta\phi_i(z) = \phi_i(z) - \phi_{i,l}. \quad (11)$$

The molar density for a positive γ ion is thus given by

$$\eta_{\gamma^+,i}(z) = \eta_{\gamma^+,i,l}\exp^{\left(\frac{-eZ_{\gamma^+}\Delta\phi_i(z)}{KT}\right)}, \quad (12)$$

and for a negative γ ion

$$\eta_{\gamma^-,i}(z) = \eta_{\gamma^-,i,l}\exp^{\left(\frac{eZ_{\gamma^-}\Delta\phi_i(z)}{KT}\right)}, \quad (13)$$

where

$$Z_\gamma = |V_\gamma|. \quad (14)$$

Equations (12) and (13) are the Boltzmann distribution of charges due to the presence of positive and negative γ ions [15], respectively, in the phases adjacent to the bilayer. Substituting Eqs. (12) and (13) in Eq. (4), we obtain

$$\frac{d^2\phi_i(z)}{dz^2} = -\frac{4\pi}{\epsilon_i}\times\left(\sum_{\gamma^+} eZ_{\gamma^+}\eta_{\gamma^+,i,l}\exp^{\left(\frac{-eZ_{\gamma^+}\Delta\phi_i(z)}{KT}\right)} - \sum_{\gamma^-} eZ_{\gamma^-}\eta_{\gamma^-,i,l}\exp^{\left(\frac{eZ_{\gamma^-}\Delta\phi_i(z)}{KT}\right)}\right) + a_i. \quad (15)$$

In the bulk regions, we can consider the electroneutrality condition

$$\sum_{\gamma^+} eZ_{\gamma^+}\eta_{\gamma^+,i,l} = \sum_{\gamma^-} eZ_{\gamma^-}\eta_{\gamma^-,i,l}, \quad (16)$$

and, in a first approximation, we assume a symmetric electrolyte to simplify our calculations, so that

$$\eta_{\gamma^+,i,l} = \eta_{\gamma^-,i,l} = \eta_{\gamma,i,l}. \quad (17)$$

We have taken the boundary values from experimental measurements in the bulk regions and on surface S_{eg}, so that $\phi_{ext,l} = \phi_{-\infty}$, $\phi_{c,l} = \phi_{+\infty}$, and $\phi_{g,l} = \phi_{S_{eg}}$. For the ionic concentrations, $\eta_{\gamma,ext,l} = \eta_{\gamma,-\infty}$, $\eta_{\gamma,c,l} = \eta_{\gamma,+\infty}$, and $\eta_{\gamma,g,l} = \eta_{\gamma,g}(-h_g - h/2)$. Throughout, we denote by $\phi_{S_{ij}}$ the electric potential on surface S_{ij} between regions i and j.

We can now use Eq. (17) to rewrite Eq. (15) as

$$\frac{d^2\phi_i(z)}{dz^2} = -\sum_{\gamma}\frac{4\pi e Z_\gamma \eta_{\gamma,i,l}}{\epsilon_i} \times\left(\exp^{\left(\frac{-eZ_\gamma\Delta\phi_i(z)}{KT}\right)} - \exp^{\left(\frac{eZ_\gamma\Delta\phi_i(z)}{KT}\right)}\right)+a_i. \quad (18)$$

If we consider that

$$\exp^{\left(\frac{-eZ_\gamma\Delta\phi_i(z)}{KT}\right)} - \exp^{\left(\frac{eZ_\gamma\Delta\phi_i(z)}{KT}\right)} = -2\sinh\left(\frac{eZ_\gamma\Delta\phi_i(z)}{KT}\right), \quad (19)$$

we can write Eq. (18) as

$$\frac{d^2\phi_i(z)}{dz^2} = \sum_{\gamma}\left(\frac{8\pi e Z_\gamma \eta_{\gamma,i,l}}{\epsilon_i}\sinh\left[\frac{eZ_\gamma\Delta\phi_i(z)}{KT}\right]\right)+a_i. \quad (20)$$

Our model only considers mono ($Z_1=1$) and divalent ($Z_2=2$) ions [4]. We thus limit the γ sum to

$$\frac{d^2\phi_i(z)}{dz^2} = \left[\frac{8\pi e\eta_{1,i,l}}{\epsilon_i}\right]\sinh\left(\frac{e\Delta\phi_i(z)}{KT}\right) + \left[\frac{16\pi e\eta_{2,i,l}}{\epsilon_i}\right]\sinh\left(\frac{2e\Delta\phi_i(z)}{KT}\right)+a_i. \quad (21)$$

To simplify further calculations, we denote

$$A_i = \frac{8\pi e\eta_{1,i,l}}{\epsilon_i},\ B_i = \frac{16\pi e\eta_{2,i,l}}{\epsilon_i}, \beta = \frac{e}{KT}, \quad (22)$$

and Eq. (21) may be expressed as

$$\frac{d^2\phi_i(z)}{dz^2} = A_i\sinh(\beta\Delta\phi_i(z)) + B_i\sinh(2\beta\Delta\phi_i(z))+a_i. \quad (23)$$

Considering that

$$\sinh(2\beta\Delta\phi_i(z)) = 2\sinh(\beta\Delta\phi_i(z))\cosh(\beta\Delta\phi_i(z)), \quad (24)$$

Eq. (23) can be rewritten as

$$\frac{d^2\phi_i(z)}{dz^2} = A_i\sinh(\beta\Delta\phi_i(z)) + 2B_i\sinh(\beta\Delta\phi_i(z))\cosh(\beta\Delta\phi_i(z))+a_i. \quad (25)$$

Multiplying Eq. (25) by

$$2d\phi_i = 2\frac{d\phi_i(z)}{dz}dz, \quad (26)$$

and integrating, we have

$$\int 2\frac{d^2\phi_i(z)}{dz^2}\frac{d\phi_i(z)}{dz}dz = \int 2A_i\sinh(\beta\Delta\phi_i(z))d\phi_i + \int 4B_i\sinh(\beta\Delta\phi_i(z))\cosh(\beta\Delta\phi_i(z))d\phi_i + \int 2a_i d\phi_i, \quad (27)$$

whose solution is

$$\left(\frac{d\phi_i(z)}{dz}\right)^2 = \frac{2A_i\cosh(\beta\Delta\phi_i(z))}{\beta} + \frac{2B_i\cosh^2(\beta\Delta\phi_i(z))}{\beta} + 2a_i\phi_i(z) + W_i, \quad (28)$$

where W_i is a constant of integration for region i.

To further simplify the symbolic representation of the equations, considering Eqs. (5) and (22), we denote

$$Q_{m_i} = 2A_i,\ Q_{d_i} = 2B_i,\ and,\ g_i = 2a_i, \quad (29)$$

where Q_{m_i} and Q_{d_i} express the influence of boundary value concentrations of monovalent and divalent ions, respectively, in each region i. Eq. (28) is thus expressed as

$$\left(\frac{d\phi_i(z)}{dz}\right)^2 = \frac{Q_{m_i}\cosh(\beta\Delta\phi_i(z))}{\beta} + \frac{Q_{d_i}\cosh^2(\beta\Delta\phi_i(z))}{\beta} + g_i\phi_i(z) + W_i. \quad (30)$$

We can rewrite Eq. (30) as

$$\frac{d\phi_i(z)}{dz} = \sqrt{\xi_i(z) + g_i\phi_i(z) + W_i}, \quad (31)$$

where

$$\xi_i(z) = \frac{Q_{m_i}\cosh(\beta\Delta\phi_i(z))}{\beta} + \frac{Q_{d_i}\cosh^2(\beta\Delta\phi_i(z))}{\beta}. \quad (32)$$

Equation (31) is the Poisson-Boltzmann equation for the electric potential in any region i.

Solution of the Poisson-Boltzmann Equation for the Extracellular Region. ($i=ext$)

In the extracellular region, the effect of fixed charges is negligible ($\rho_{fext}=0$ and $g_{ext}=0$), and the solution of Eq. (31) therefore only considers the electrolytic charges. Moreover, the electric potential in $z=-\infty$ is constant and we can write

$$\left.\frac{d\phi_{ext}(z)}{dz}\right|_{(z=-\infty)} = 0. \quad (33)$$

In order to use Eq. (31) to calculate the potential in the extracellular region, we must find the value of W_{ext}. We thus consider an imaginary surface $S_{-\infty}$, perpendicular to the $z-$axis, at $z_1 \ll (-h_g - h/2)$, where $\rho_{fext}=0$. We then integrate Eq. (31) from another position $z_2 < z_1$ to z_1. Since both z_1 and z_2 are in the $-\infty$ region, $\phi_{-\infty} = \phi_{ext}(z_1) = \phi_{ext}(z_2) = \phi_{S_{-\infty}}$, and $\Delta\phi_{ext}(z_2) = \phi_{ext}(z_2) - \phi_{S_{-\infty}} = 0$. We can then substitute Eq. (33)

and $\Delta\phi_{ext}(z_2)=0$ in Eq. (31), to calculate W_{ext} as

$$0=\frac{Q_{m_{ext}}}{\beta}\cosh(0)+\frac{Q_{d_{ext}}}{\beta}\cosh^2(0)+W_{ext}, \tag{34}$$

and

$$W_{ext}=\frac{-Q_{m_{ext}}-Q_{d_{ext}}}{\beta}. \tag{35}$$

We then substitute Eq. (35) in Eq. (31) to obtain the differential equation for $\phi_{ext}(z)$, for any position $z<(-h_g-h/2)$, in the extracellular region

$$\frac{d\phi_{ext}(z)}{dz}=\sqrt{\lambda_{ext}(z)+\sigma_{ext}(z)}, \tag{36}$$

where

$$\begin{aligned}\lambda_{ext}(z)&=\frac{Q_{m_{ext}}[\cosh(\beta\Delta\phi_{ext}(z))-1]}{\beta},\\ \sigma_{ext}(z)&=\frac{Q_{d_{ext}}\left[\cosh^2(\beta\Delta\phi_{ext}(z))-1\right]}{\beta},\\ &and,\ \Delta\phi_{ext}(z)=\phi_{ext}(z)-\phi_{-\infty}.\end{aligned} \tag{37}$$

Equation (36) can be simplified to

$$\frac{d\phi_{ext}(z)}{dz}=\sqrt{\chi_{ext}(z)+\omega_{ext}(z)}, \tag{38}$$

where

$$\begin{aligned}\chi_{ext}(z)&=2\frac{Q_{m_{ext}}\sinh^2\left(\frac{\beta}{2}\Delta\phi_{ext}(z)\right)}{\beta},\\ &and,\\ \omega_{ext}(z)&=\frac{Q_{d_{ext}}\sinh^2(\beta\Delta\phi_{ext}(z))}{\beta}.\end{aligned} \tag{39}$$

Solution of the Poisson-Boltzmann Equation for the Cytoplasmic Region. $(i=c)$Because, in the cytoplasmic region, the potential in $z=+\infty$ is also constant,

$$\left.\frac{d\phi_c(z)}{dz}\right|_{(z=+\infty)}=0. \tag{40}$$

As we did for the extracellular region, to calculate the potential in the cytoplasmic region using Eq. (31), we must first find the value of W_c. We thus consider an imaginary surface $S_{+\infty}$, perpendicular to the $z-$axis, at $z_3\gg(h/2)$. We then integrate Eq. (31) from another position $z_4>z_3$ to z_3. As both z_3 and z_4 are in the $+\infty$ region, $\phi_{+\infty}=\phi_c(z_3)=\phi_c(z_4)=\phi_{S_{+\infty}}$, and $\Delta\phi_c(z_4)=\phi_c(z_4)-\phi_{S_{+\infty}}=0$. We thus substitute Eq. (40) and $\Delta\phi_c(z_4)=0$ in Eq. (31), to obtain W_c as

$$0=\frac{Q_{m_c}}{\beta}\cosh(0)+\frac{Q_{d_c}}{\beta}\cosh^2(0)+g_c\phi_{+\infty}+W_c. \tag{41}$$

The constant of integration W_c is

$$W_c=\frac{-Q_{m_c}-Q_{d_c}}{\beta}-g_c\phi_{+\infty}. \tag{42}$$

We then substitute Eq. (42) in Eq. (31) to obtain the differential equation for $\phi_c(z)$, for any $z>(h/2)$, in the cytoplasmic region

$$\frac{d\phi_c(z)}{dz}=\sqrt{\lambda_c(z)+\sigma_c(z)+g_c\Delta\phi_c(z)}, \tag{43}$$

where

$$\begin{aligned}\lambda_c(z)&=\frac{Q_{m_c}[\cosh(\beta\Delta\phi_c(z))-1]}{\beta},\\ \sigma_c(z)&=\frac{Q_{d_c}\left[\cosh^2(\beta\Delta\phi_c(z))-1\right]}{\beta},\\ &and,\ \Delta\phi_c(z)=\phi_c(z)-\phi_{+\infty}.\end{aligned} \tag{44}$$

Equation (43) can be simplified to

$$\frac{d\phi_c(z)}{dz}=\sqrt{\chi_c(z)+\omega_c(z)+g_c\Delta\phi_c(z)}, \tag{45}$$

where

$$\begin{aligned}\chi_c(z)&=2\frac{Q_{m_c}\sinh^2\left(\frac{\beta}{2}\Delta\phi_c(z)\right)}{\beta},\ and,\\ \omega_c(z)&=\frac{Q_{d_c}\sinh^2(\beta\Delta\phi_c(z))}{\beta}.\end{aligned} \tag{46}$$

Solution of the Poisson-Boltzmann Equation for the Glycocalyx Region. $(i=g)$We consider that the potential $\phi_{S_{eg}}$ on the surface S_{eg} satisfies

$$\left.\frac{d\phi_g(z)}{dz}\right|_{(z=-h_g-h/2)}\hat{z}=\vec{E}_g|_{S_{eg}}, \tag{47}$$

where $\hat{z}$ is the unit vector in the z direction, and $\vec{E}_k|_{S_{ij}}$ is the electric field in region k, $\vec{E}_k(z_{ij})$, at z_{ij}, the position of surface S_{ij} between regions i and j, e.g., $\vec{E}_g|_{S_{eg}}=\vec{E}_g(-h_g-h/2)$ is the electric field in the glycocalyx region at the position of surface S_{eg}.

We have previously stated that the boundary condition for ionic concentrations in the glycocalyx is defined as $\eta_{\gamma,g,l}=\eta_{\gamma,g}(-h_g-h/2)$. In order to obtain $\eta_{\gamma,g}(-h_g-h/2)$ from the experimentally measured $\eta_{\gamma,-\infty}$, we would need to apply Eqs. (12) and (13). This would result in four values of $\eta_{\gamma,g}(-h_g-h/2)$ (for positive and negative, monovalent and divalent ions). In this case, the symmetric electrolytes assumption (Eq. (17)) would not hold, and the mathematical formalism leading to Eq. (31) would not apply. Nevertheless, in Eq. (15), the difference in the contributions of the terms involving $\eta_{\gamma,g,l}$ for the different ions is small compared to the value of the a_i term, which is a few order of magnitude larger. We thus assume that $\eta_{\gamma,g}(-h_g-h/2)=\eta_{\gamma,-\infty}$, for monovalent and divalent ions.

In order to use Eq. (31) to calculate the potential in the glycocalyx region, we need to find the value of W_g. We thus solve

Eq. (31) at $z=-h_g-h/2$, on the surface S_{eg}, and take $\phi_g(-h_g-h/2)=\phi_{S_{eg}}$, and $\Delta\phi_g(-h_g-h/2)=\phi_g(-h_g-h/2)-\phi_{S_{eg}}=0$. We can then substitute Eq. (47) and $\Delta\phi_g(-h_g-h/2)=0$ in Eq. (31), to calculate W_g as

$$\left(\vec{E}_g|_{S_{eg}}\right)^2=\frac{Q_{mg}}{\beta}\cosh(0)+\frac{Q_{dg}}{\beta}\cosh^2(0)+g_g\phi_{S_{eg}}+W_g. \quad (48)$$

The constant of integration W_g, for the glycocalyx region, is therefore

$$W_g=\left(\vec{E}_g|_{S_{eg}}\right)^2-\left(\frac{Q_{mg}+Q_{dg}}{\beta}\right)-g_g\phi_{S_{eg}}. \quad (49)$$

We then substitute Eq. (49) in Eq. (31) to obtain the differential equation for $\phi_g(z)$, for any position $(-h_g-h/2)<z<(-h/2)$, in the glycocalyx region

$$\frac{d\phi_g(z)}{dz}=\sqrt{\lambda_g(z)+\sigma_g(z)+g_g\Delta\phi_g(z)+\vec{E}_g|^2_{S_{eg}}}, \quad (50)$$

where

$$\begin{aligned}\lambda_g(z)&=\frac{Q_{mg}\left[\cosh\left(\beta\Delta\phi_g(z)\right)-1\right]}{\beta},\\ \sigma_g(z)&=\frac{Q_{dg}\left[\cosh^2\left(\beta\Delta\phi_g(z)\right)-1\right]}{\beta},\\ &and,\ \Delta\phi_g(z)=\phi_g(z)-\phi_{S_{eg}}.\end{aligned} \quad (51)$$

Equation (50) can be further simplified to

$$\frac{d\phi_g(z)}{dz}=\sqrt{\chi_g(z)+\omega_g(z)+g_g\Delta\phi_g(z)+\vec{E}_g|^2_{S_{eg}}}, \quad (52)$$

where

$$\begin{aligned}\chi_g(z)&=2\frac{Q_{mg}\sinh^2\left(\frac{\beta}{2}\Delta\phi_g(z)\right)}{\beta},\ and,\\ \omega_g(z)&=\frac{Q_{dg}\sinh^2\left(\beta\Delta\phi_g(z)\right)}{\beta}.\end{aligned} \quad (53)$$

Solution of the Poisson-Boltzmann Equation for the Bilayer. $(i=b)$As mentioned earlier, because the bilayer is highly hydrophobic, $\rho_b(z)=0$, and therefore Eq. (2) assumes the form

$$\nabla^2\phi_b(x,y,z)=0, \quad (54)$$

and its solution is a family of linear functions. The electric field within the bilayer (see Eq. (59)), $\vec{E}_b$, can thus be expressed as

$$\vec{E}_b=\frac{\phi_{S_{gb}}-\phi_{S_{bc}}}{h}\hat{z}. \quad (55)$$

Surface Potentials

In order to solve the differential Eqs. (38), (45) and (52) for the extracellular, cytoplasmic and glycocalyx regions of the neuronal membrane, respectively, we must know the values of the surface potentials $\phi_{S_{eg}}$, $\phi_{S_{gb}}$ and $\phi_{S_{bc}}$. Although membrane surface potentials in cells cannot be measured experimentally, it is possible to obtain analytical predictions for the values of $\phi_{S_{eg}}$, $\phi_{S_{gb}}$ and $\phi_{S_{bc}}$, from basic electrostatic relations, as we will now show.

Considering the surface densities of electric charges, Gauss' law, and the discontinuity of the electric field vector on the surfaces S_{eg}, S_{gb} and S_{bc}, we obtain

$$\epsilon_g\vec{E}_g|_{S_{eg}}-\epsilon_{ext}\vec{E}_{ext}|_{S_{eg}}=4\pi Q_{S_{eg}}\hat{z}, \quad (56)$$

$$\epsilon_b\vec{E}_b|_{S_{gb}}-\epsilon_g\vec{E}_g|_{S_{gb}}=4\pi Q_{S_{gb}}\hat{z},\ and, \quad (57)$$

$$\epsilon_c\vec{E}_c|_{S_{bc}}-\epsilon_b\vec{E}_b|_{S_{bc}}=4\pi Q_{S_{bc}}\hat{z}, \quad (58)$$

respectively, where $\vec{E}_b|_{S_{gb}}=\vec{E}_b|_{S_{bc}}=\vec{E}_b$ (see Eq. (55)). In the above, $Q_{S_{eg}}$, $Q_{S_{gb}}$ and $Q_{S_{bc}}$ stand for the charge density on the S_{eg}, S_{gb} and S_{bc} surfaces, respectively.

As

$$\vec{E}_i=-\vec{\nabla}\phi_i(z)=-\frac{d\phi_i(z)}{dz}\hat{z}, \quad (59)$$

in order to determine the discontinuity of the electric field vector on the surfaces S_{eg}, S_{gb} and S_{bc}, we substitute Eq. (59) in Eqs. (56), (57) and (58), and obtain

$$\vec{E}_g|_{S_{eg}}=\frac{4\pi Q_{S_{eg}}-\epsilon_{ext}\frac{d\phi_{ext}(z)}{dz}|_{(z=-h_g-h/2)}}{\epsilon_g}\hat{z}, \quad (60)$$

$$\vec{E}_b=\frac{4\pi Q_{S_{gb}}-\epsilon_g\frac{d\phi_g(z)}{dz}|_{(z=-h/2)}}{\epsilon_b}\hat{z},\ and, \quad (61)$$

$$\vec{E}_b=\frac{-4\pi Q_{S_{bc}}-\epsilon_c\frac{d\phi_c(z)}{dz}|_{(z=h/2)}}{\epsilon_b}\hat{z}. \quad (62)$$

As we have previously obtained the expression that determines the electric field within the bilayer, $\vec{E}_b$, we substitute Eq. (55) into Eqs. (61) and (62), and obtain

Table 1. Values of simulation parameters for both the spinal ganglion neuron and the neuroblastoma cell.

Parameter	Symbol	Value	Value in CGS	References
Dielectric constant in region b	ϵ_b	2	2	[3,4]
Dielectric constant in region i ($i=ext,g,c$)	ϵ_i	81	81	[4]
Glycocalyx width	h_g	2.5 nm	2.50×10^{-7} cm	[4,9,16]
Bilayer thickness	h	7.5 nm	7.50×10^{-7} cm	[3,4,9,16]
Concentration of monovalent ions in bulk extracellular region	$\eta_{1,-\infty}$	0.154 M	9.27×10^{19} cm^{-3}	[16,17,29,30]
Concentration of monovalent ions on S_{eg}	$\eta_{1,S_{eg}}$	0.154 M	9.27×10^{19} cm^{-3}	[16,17,29,30]
Concentration of divalent ions in bulk extracellular region	$\eta_{2,-\infty}$	0.002 M	1.20×10^{18} cm^{-3}	[16,17,29,30]
Concentration of divalent ions on S_{eg}	$\eta_{2,S_{eg}}$	0.002 M	1.20×10^{18} cm^{-3}	[16,17,29,30]
Concentration of monovalent ions in bulk cytoplasmic region	$\eta_{1,+\infty}$	0.154 M	9.27×10^{19} cm^{-3}	[29–31]
Concentration of divalent ions in bulk cytoplasmic region	$\eta_{2,+\infty}$	0.0004 M	2.41×10^{17} cm^{-3}	[29,30]
Potential in $-\infty$, the extracellular region	$\phi_{-\infty}$	0 mV	0 statV	[3,4]
Temperature	T	310 K	310 K	[4]
Boltzmann's constant	K	1.38×10^{-23} J/K	1.38×10^{-16} erg/K	[32]
Absolute value of electron charge	e	1.60×10^{-19} C	4.80×10^{-10} statC	[32]
Viscosity of region i	v_i	0.1 Pa·s	1 P	[3]

[1]CGS is the centimeter-gram-second system of units.

doi:10.1371/journal.pone.0096194.t001

$$\phi_{S_{bc}}=\phi_{S_{gb}}-\frac{h}{\epsilon_b}\left(4\pi Q_{S_{gb}}-\epsilon_g\frac{d\phi_g(z)}{dz}|_{(z=-h/2)}\right), \quad (63)$$

$$\phi_{S_{gb}}=\phi_{S_{bc}}-\frac{h}{\epsilon_b}\left(4\pi Q_{S_{bc}}+\epsilon_c\frac{d\phi_c(z)}{dz}|_{(z=h/2)}\right), \quad (64)$$

respectively.

Substituting Eqs. (52) and (60) in Eq. (63), we determine the expression to calculate the surface potential $\phi_{S_{bc}}$

$$\phi_{S_{bc}}=\phi_{S_{gb}}-\frac{4\pi Q_{S_{gb}}h}{\epsilon_b}+\frac{\epsilon_g h}{\epsilon_b}\sqrt{\alpha}, \quad (65)$$

where

$$\alpha=\chi_g(-h/2)+\omega_g(-h/2)+g_g\Delta\phi_g(-h/2)+\left(\frac{4\pi Q_{S_{eg}}-\epsilon_{ext}\frac{d\phi_{ext}(z)}{dz}|_{(z=-h_g-h/2)}}{\epsilon_g}\right)^2 \quad (66)$$

and here, $\Delta\phi_g(-h/2)=\phi_{S_{gb}}-\phi_{S_{eg}}$. In the same manner, substituting Eq. (45) in Eq. (64), we determine the expression to calculate the surface potential $\phi_{S_{gb}}$

$$\phi_{S_{gb}}=\phi_{S_{bc}}-\frac{4\pi Q_{S_{bc}}h}{\epsilon_b}-\frac{\epsilon_c h}{\epsilon_b}\sqrt{\kappa}, \quad (67)$$

where

$$\kappa=\chi_c(h/2)+\omega_c(h/2)+g_c\Delta\phi_c(h/2), \quad (68)$$

and here, $\Delta\phi_c(h/2)=\phi_{S_{bc}}-\phi_{+\infty}$.

The electric potential on the surface S_{eg}, $\phi_{S_{eg}}$, is determined from electrophoretic experiments [9,16,17] and the Helmholtz-Smoluchowski equation [3]

$$\mu=\frac{\epsilon_i\zeta_i}{4\pi v_i}, \quad (69)$$

where μ is the electrophoretic mobility, $\zeta_i=\phi_{S_{eg}}-\phi_{-\infty}$ is the zeta potential, and v_i is the viscosity of region i. As, in our model, we define the potential $\phi_{-\infty}=0$, the surface potential $\phi_{S_{eg}}$ is

$$\phi_{S_{eg}}=\frac{4\pi v_i\mu}{\epsilon_i}. \quad (70)$$

Model Calculations for Spinal Ganglion Neurons and Neuroblastoma Cells

We have used data obtained from experimental observations [9,16,17] for values of parameters, in order to solve the first order ordinary differential equations, obtained from the Poisson-Boltzmann Eq. (31), for the different regions of the membrane. Some experimental values were obtained from electrophoretic experiments. Since each kind of cell presents a specific electrophoretic mobility, the values of some parameters are different for the spinal ganglion neuron and the neuroblastoma cell, in our calculations. Tables (1) and (2) show all experimental values of the parameters used to solve the equations for the ganglion and the neuroblastoma. The difference $\phi_{+\infty}-\phi_{-\infty}$ is called the transmembrane potential and is denoted as ϕ_R in the resting state, and ϕ_A in the AP state. We have defined $\phi_{-\infty}=0$ in our calculations,

so that $\phi_R = \phi_{+\infty}$ in the resting state, and $\phi_A = \phi_{+\infty}$ in the AP state. We have thus examined the influence of parameters that represent electrical properties of the membrane, on the resting and AP states, and analyzed the differences between the healthy spinal ganglion neuron and the neuroblastoma cell.

We implemented an approximate heuristic for finding roots of functions, to calculate $\phi_{S_{gb}}$ and $\phi_{S_{bc}}$ from Eqs. (65) and (67), which is specified in the next subsection. As mentioned earlier, the potential $\phi_{S_{eg}}$ was calculated with Eq. (70), from data obtained from electrophoretic experiments.

As we included the density of charges fixed onto proteins within the membrane regions in the Poisson Eq. (1), we obtained a non-linear Poisson-Boltzmann Eq. (31), whose analytical solution has not been found. We therefore calculated values of the potential profiles with Eqs. (38), (45) and (52) numerically, using the Runge-Kutta method. The model simulation code is available on GitHub at https://github.com/pintotm/PLoSOne2014.

Roots of the System of Non-linear Equations. Because there is no experimental method to directly measure values of the surface potentials $\phi_{S_{gb}}$ and $\phi_{S_{bc}}$, we use Eqs. (65) and (67) that form a system of non-linear equations with two variables, $\phi_{S_{gb}}$ and $\phi_{S_{bc}}$, to determine these values. Some research work [3,4,9,16,17] indicates that the values of these potentials in real cells are in a limited region of the $\phi_{S_{gb}} \times \phi_{S_{bc}}$ plane. This means that we are looking for one of the roots of Eqs. (65) and (67), in a known region.

We can write the system of Eqs. (65) and (67) as

$$\begin{aligned} \phi_{S_{gb}} &= G\left(\phi_{S_{bc}}\right) \\ \phi_{S_{bc}} &= F\left(\phi_{S_{gb}}\right). \end{aligned} \tag{71}$$

Our simple method for finding the roots of this system consists in the steps described in *Algorithm_Roots*. At the resting state, $min = -250$ mV and $max = -50$ mV, while, at the AP state, $min = 10$ mV and $max = 100$ mV.

Algorithm. *Algorithm Roots*
Step 0: $\delta_{\phi_{min}} = 10^{-4}$ mV
Step 1: Choose an initial value for $\phi_{S_{bc}}$
in min $< \phi_{S_{bc}} <$ max
Step 2: $\delta_{\phi} = 20$ mV
Step 3: While $\delta_{\phi} > \delta_{\phi_{\min}}$ do
begin
$\phi_{S_{ab}}$ = G($\phi_{S_{bc}}$)
$\phi^*_{S_{bc}}$ = F($\phi_{S_{ab}}$)
If $|\phi_{S_{bc}} - \phi^2{*}_{S_{bc}}| < \delta_{\phi}$ **then**
δ_{ϕ} = $|\phi_{S_{bc}} - \phi^2{*}_{S_{bc}}|$
$\phi_{S_{bc}}$ = $\phi^2{*}_{S_{bc}}$
else
return to Step 1
end if
end While

Algorithm for determining $\phi_{S_{gb}}$ and $\phi_{S_{bc}}$, for the spinal ganglion neuron and the neuroblastoma cell. With the $\phi_{S_{bc}}$ value found with this procedure, we use Eq. (67) to obtain the corresponding $\phi_{S_{gb}}$ value. The surface potentials $\phi_{S_{gb}}$ and $\phi_{S_{bc}}$ for the spinal ganglion neuron and the neuroblastoma cell, whose values are shown in the following section, were obtained with *Algorithm_Roots*.

Results

The hydrophilic heads of the phospholipids that form the surfaces of the bilayer are negatively charged or polarized, and attribute a fixed charge density to surfaces S_{gb} and S_{bc}. In the situation of electrostatic equilibrium, which we are analyzing, both bilayer surfaces, S_{gb} and S_{bc}, are surrounded by a "diffuse electric layer" formed by the motion of free ions in the fluid ionic solution, under the influence of electric attraction and thermal motion [12–15].

It is known that the inner surface charge density ($|Q_{S_{bc}}|$) of the membrane is significantly higher than the outer surface density, due to the presence of negatively charged heads of phospholipids on the inner surface (phosphatidylserine), while on the outer surface the presence of neutral phospholipids dominates [18]. Moreover, the net charges fixed onto cytoplasmic proteins ($|\rho_{fc}|$) are considered to be higher than the fixed net charges distributed in the glycocalyx region [19–21].

With our mathematical model, we first investigate the effect of $Q_{S_{bc}}$ and ρ_{fc} on the electric potential on the surfaces of the neuronal membranes of the spinal ganglion and the neuroblastoma. However, there is little information in the literature, regarding experimentally obtained quantities related to electric charges fixed within biological membranes. This is mainly due to the difficulties involved in obtaining the experimental measurements of these quantities. We therefore examine the behavior of the potentials $\phi_{S_{gb}}$ and $\phi_{S_{bc}}$ for a range of values of the ratios $Q_{S_{bc}}/Q_{S_{eg}}$ and ρ_{fc}/ρ_{fg}, given known experimental values of $Q_{S_{eg}}$ and ρ_{fg}, i.e. $Q_{S_{bc}}$ and ρ_{fc} are multiples of $Q_{S_{eg}}$ and ρ_{fg}, respectively. We note that both glycocalyx and cytoplasm and their surfaces are negatively charged, so that $Q_{S_{eg}} < 0$, $Q_{S_{bc}} < 0$, $\rho_{fg} < 0$ and $\rho_{fc} < 0$.

Figure (2) shows the behavior of $\phi_{S_{gb}}$ and $\phi_{S_{bc}}$ as we increase the negative charge on S_{bc}, i.e. as we decrease $Q_{S_{bc}}$. We notice that for both the resting and AP states, a decrease of $Q_{S_{bc}}$ has almost no effect on the surface potentials of both neuronal membranes. These variations in $Q_{S_{bc}}$ only determine a small gradual decay of $\phi_{S_{bc}}$ during the resting state of the cells. The resting and AP states were specified by boundary conditions, i.e. specific parametric values applied to the model. Values for $\phi_{S_{gb}}$ and $\phi_{S_{bc}}$ are different between these types of cells, due to their specific membrane properties. We also observe that $\phi_{S_{gb}}$ remains constant at -34.97 mV and -25.17 mV, respectively for the spinal ganglion and neuroblastoma cells, when they switch from the resting to AP states, and vice versa. Moreover, during the AP state, $\phi_{S_{bc}}$ assumes values near the transmembrane potentials (Fig. (2B)).

We also examine the electric potential on the surfaces of the membranes of the healthy and the cancerous cells, in response to variations in the density of charges fixed onto proteins of the cytoplasm. Figure (3) presents the resulting $\phi_{S_{gb}}$ and $\phi_{S_{bc}}$ as we increase this density of negative charges in the cytoplasm, i.e. as we decrease ρ_{fc}. For both the resting and AP states, $\phi_{S_{gb}}$ remains constant when values of ρ_{fc} vary. However, a decrease in ρ_{fc} causes a substantial fall of $\phi_{S_{bc}}$, for both types of cells, at resting and AP states. At the AP state, $\vartheta_{S_{bc}}$ presents a quick drop when $\rho_{fc}/\rho_{fg} < 20$ and tends to an asymptotic value, for decreasing values of ρ_{fc}, for both types of cells.

Besides investigating the effect of fixed charges on the potential on the surfaces of these membranes, we study how the electric potential profile changes across the membranes of spinal ganglion neurons and neuroblastoma cells, for the resting and AP states. Although the values of $Q_{S_{bc}}$ and ρ_{fc} are not known, $|Q_{S_{bc}}|$ and $|\rho_{fc}|$ are much larger than the corresponding charges in the outer

Table 2. Parameter values specific to the spinal ganglion neuron (left) and to the neuroblastoma cell (right).

Parameter	Symbol	Spinal Ganglion Neuron			Neuroblastoma		
		Value	Value in CGS	Reference	Value	Value in CGS	Reference
Fixed charge density in glycocalyx	ρ_{fg}	-0.12 e/nm^3	-5.76×10^{10} statC/cm^3	[16]	-0.2 e/nm^3	-9.61×10^{10} statC/cm^3	[9]
Charge density on S_{eg}	$Q_{S_{eg}}$	-0.012 e/nm^2	-5.76×10^{2} statC/cm^2	[16]	-0.02 e/nm^2	-9.61×10^{2} statC/cm^2	[9]
Charge density on S_{gb}	$Q_{S_{gb}}$	$-1/1000$ e/A^2	-4.80×10^{3} statC/cm^2	[33]	$-1/385$ e/A^2	-1.25×10^{4} statC/cm^2	[33]
Electric potential on S_{eg}	$\phi_{S_{eg}}$	-19.52 mV	-6.51×10^{-5} statV	Eq. (70)	-25.10 mV	-8.37×10^{-5} statV	Eq. (70)
Resting transmembrane potential	ϕ_R	-69 mV	-2.30×10^{-4} statV	[16,34]	-64 mV	-2.13×10^{-4} statV	[10]
Action transmembrane potential	ϕ_A	40 mV	1.33×10^{-4} statV	[35]	30 mV	1.00×10^{-4} statV	[36]
Electrophoretic mobility	μ	-1.40 mm.cm/V.s	-4.20×10^{-4} cm^2/statV.s	[9,16]	-1.80 mm.cm/V.s	-5.40×10^{-4} cm^2/statV.s	[9]

doi:10.1371/journal.pone.0096194.t002

regions. We thus chose fixed values of $Q_{S_{bc}}=30Q_{S_{eg}}$ and $\rho_{fc}=20\rho_{fg}$ (which are the same fixed values in Figs. (3) and (2), respectively) to calculate the potential profile in Fig. (4), for the resting state and in Fig. (5), during the AP state. For both natural states of these cells, we verify an accentuated decrease of the potential along the z axis, from the extracellular region to the surface of the glycocalyx. This decay is slightly more substantial for the neuroblastoma than for the spinal ganglion neuron, although the shapes of both curves are very similar.

In the spinal ganglion neuron, the potential maintains a substantial drop across the glycocalyx. Interestingly, this phenomenon does not occur for the cancerous cells, whose electric potential remains almost unchanged in this region. We observe linear variations of the potential across the bilayer of these cells, for both resting and AP states. During rest, the electric potential assumes much lower values on S_{bc} than the asymptotic value in the bulk cytoplasmic region, while during the AP state, these values are similar. Before reaching the transmembrane potential value, the intracellular potential exponentially increases from the inner surface of the membrane to the bulk cytoplasmic region, during the resting condition, while during the AP state, we see no alteration in the electric potential in the cytoplasm, for both cells.

Discussion

There are other membrane phenomena due to electric charge effects that we have not considered in our model, such as the electric pump current [22]. We have not included these phenomena here as they seem to be negligible, in a first approximation, to the determination of the electric surface potentials. For example, Jäckle [22] states that ''the net electric pump current is not a relevant parameter in the casual theory of the resting potential''.

Experiments have revealed important discrepancies in the electrical properties of spinal ganglion neurons and neuroblastoma cells [9,16]. These differences are reflected in the parameter values we used in our simulations, as shown in Table (2). We notice that the values for the electrophoretic mobility, and the charge densities in the glycocalyx and on S_{eg} are much more negative for the neuroblastoma than for the ganglion. Because neuroblastoma cells contain a higher amount of negative ρ_{fg}, $Q_{S_{eg}}$ and μ compared with ganglion neurons, we indeed expected to obtain lower $\phi_{S_{eg}}$ and $\phi_{S_{bc}}$ values for the neuroblastoma in our simulations.

Our simulations also demonstrate that variations in the electric charges fixed onto the inner surface of the membrane have a small effect on the electric potential of the surfaces that compose the neuronal membranes (Fig. (2)). We observe only a gentle gradual drop in $\phi_{S_{bc}}$ of the spinal ganglion and the neuroblastoma cells during the resting state, as charges fixed on S_{bc} decrease (more negative values). However, our model shows that decreasing the density of charges fixed onto proteins of the cytoplasm (increasing $|\rho_{fc}|$ and ρ_{fc}/ρ_{fg}) results in a substantial decay of $\phi_{S_{bc}}$, in both cells (Fig. (3)).

Nonetheless, variations of intracellular charges fixed on the membrane and on the cytoplasmic proteins have no effect on the potential on S_{gb} (Figs. (2) and (3)). This is related to the fact that the membrane plays a role in electrically isolating the intracellular and extracellular regions, due to the absence of charges within the lipidic bilayer (see Eq. (54)).

The results we obtained for the spinal ganglion neurons and the neuroblastoma cells are generally similar to those obtained for the squid axon membrane in [4]. These authors showed that a decrease of $Q_{S_{bc}}$ provokes a gentle decrease of $\phi_{S_{bc}}$ of the squid

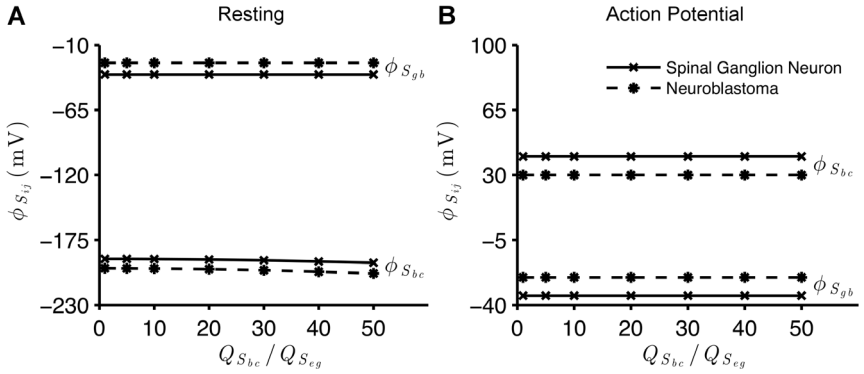

Figure 2. Sensitivity of the membrane surface potentials to inner surface charge density. Electric potential on the surfaces of regions of the membranes of the spinal ganglion neuron ($\times$) and the neuroblastoma cell ($*$), as a function of the ratio $Q_{S_{bc}}/Q_{S_{eg}}$, as $Q_{S_{eg}}$ is kept constant. In the resting state (A), $\phi_{S_{bc}} = -190.97$ mV, for the ganglion neuron and $\phi_{S_{bc}} = -198.97$ mV, for the neuroblastoma, when $Q_{S_{bc}}/Q_{S_{eg}} = 1$ (maximum values), while $\phi_{S_{bc}} = -194.25$ mV (ganglion) and $\phi_{S_{bc}} = -203.30$ mV (neuroblastoma), for $Q_{S_{bc}}/Q_{S_{eg}} = 50$ (minimum). In the AP state (B), $\phi_{S_{bc}} = 39.99$ mV, for the ganglion neuron and $\phi_{S_{bc}} = 29.99$ mV, for the neuroblastoma, when $Q_{S_{bc}}/Q_{S_{eg}} = 1$ (maximum), while $\phi_{S_{bc}} = 39.97$ mV (ganglion) and $\phi_{S_{bc}} = 29.97$ mV (neuroblastoma) for $Q_{S_{bc}}/Q_{S_{eg}} = 50$ (minimum). In all simulations, for resting and AP states, $\phi_{S_{gb}} = -34.97$ mV, for the ganglion, and $\phi_{S_{gb}} = -25.17$ mV, for the neuroblastoma. In both graphs, $\rho_{fc} = 20\rho_{fg}$.
doi:10.1371/journal.pone.0096194.g002

axon membrane. This behavior was also observed in our simulations for the membranes of spinal ganglion neurons and neuroblastoma cells. Nevertheless, their results indicate that a decrease of $Q_{S_{bc}}$ causes a sensitive increase of $\phi_{S_{gb}}$ during the AP state and a small decrease of $\phi_{S_{gb}}$ during the resting state, whereas our results show a constant $\phi_{S_{gb}}$ value for ganglion and neuroblastoma cells. The insensitivity of $\phi_{S_{gb}}$ to variations of $Q_{S_{bc}}$ which we have found seems more reasonable, given the above mentioned isolating effect of the lipidic bilayer.

Cortez and collaborators [4] have shown that a decrease of ρ_{fc} (in the same range of ρ_{fc}/ρ_{fg} which we studied) causes practically no change in the surface potentials. A possible reason for this may be that the ρ_{fg} value for the squid axon is approximately zero, so that the values of ρ_{fc}, in the domain of their graphs, are very close to zero. In contrast, our simulations indicate that a decrease of ρ_{fc} provokes an expressive fall of $\phi_{S_{bc}}$. In our case, ρ_{fg} (and ρ_{fc}) values for ganglion neurons and neuroblastoma cells are much more negative than those observed for squid axons and, therefore, a decrease of ρ_{fc} has a high influence on $\phi_{S_{bc}}$.

An interesting result of our calculations is that, in the spinal ganglion neuron, the electric potential across the glycocalyx decreases, and this does not occur in the neuroblastoma cell. This reveals an important discrepancy of the electric fields in the glycocalyx of both types of cells (Figs. (4) and (5)), and may explain the difference between their electrophoretic behavior, which was observed in experiments [9,16]. As expected, the electric potential presents a linear behavior within the bilayer of the membrane during the resting and AP states, due to the absence of electric charges in this region.

The strong negative electric potential on S_{bc} is a characteristic of the potential profile in the resting state, and this probably occurs for all types of neuronal cells (Fig. (4)). The steep increase of the potential from S_{bc} towards the bulk cytoplasmic region is regulated

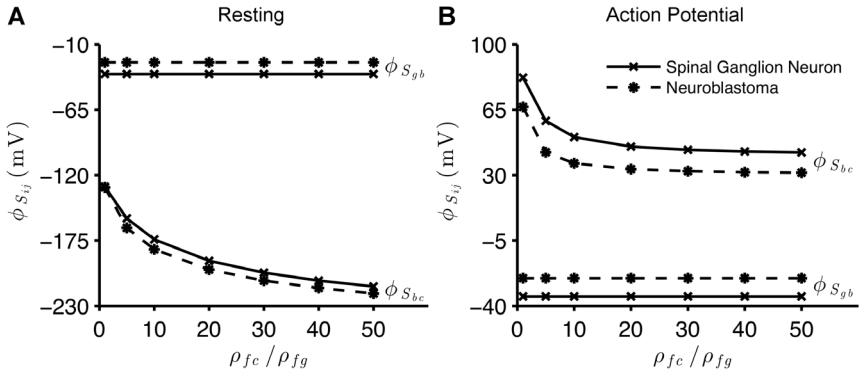

Figure 3. Sensitivity of the membrane surface potentials to charge density in the cytoplasm. Electric potentials $\phi_{S_{gb}}$ and $\phi_{S_{bc}}$ as a function of ρ_{fc}/ρ_{fg}, as ρ_{fg} is kept constant, for the spinal ganglion neuron ($\times$) and the neuroblastoma cell ($*$). In the resting state (A), $\phi_{S_{bc}} = -129.63$ mV, for the ganglion neuron and $\phi_{S_{bc}} = -130.36$ mV, for the neuroblastoma, when $Q_{S_{bc}}/Q_{S_{eg}} = 1$ (maximum values), while $\phi_{S_{bc}} = -213.74$ mV (ganglion) and $\phi_{S_{bc}} = -219.56$ mV (neuroblastoma), for $Q_{S_{bc}}/Q_{S_{eg}} = 50$ (minimum). In the AP state (B), $\phi_{S_{bc}} = 82.26$ mV, for the ganglion neuron and $\phi_{S_{bc}} = 66.57$ mV, for the neuroblastoma, when $Q_{S_{bc}}/Q_{S_{eg}} = 1$ (maximum), while $\phi_{S_{bc}} = 42.13$ mV (ganglion) and $\phi_{S_{bc}} = 31.28$ mV (neuroblastoma) for $Q_{S_{bc}}/Q_{S_{eg}} = 50$ (minimum). In all simulations, for resting and AP states, $\phi_{S_{gb}} = -34.97$ mV, for the ganglion, and $\phi_{S_{gb}} = -25.17$ mV, for the neuroblastoma. In both graphs, $Q_{S_{bc}} = 30Q_{S_{eg}}$.
doi:10.1371/journal.pone.0096194.g003

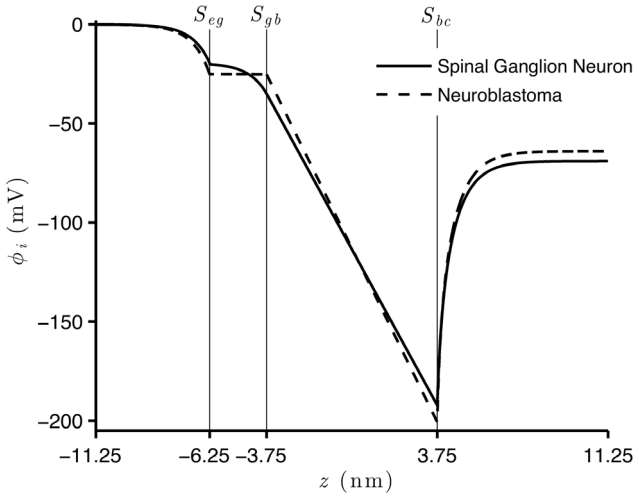

Figure 4. Electric potential across the membranes of spinal ganglion neurons and neuroblastoma cells, during resting state. Solutions of Eq. (52) with boundary $\phi_{S_{eg}}$, and Eq. (45) with boundary $\phi_{+\infty}=\phi_R$ result respectively in $\phi_{S_{gb}}=-34.97$ mV and $\phi_{S_{bc}}=-192.22$ mV, for the spinal ganglion neuron (solid), and for the neuroblastoma cell (dashed) in $\phi_{S_{gb}}=-25.17$ mV and $\phi_{S_{bc}}=-200.66$ mV. For all simulations, $Q_{S_{bc}}=30Q_{S_{eg}}$ and $\rho_{fc}=20\rho_{fg}$.
doi:10.1371/journal.pone.0096194.g004

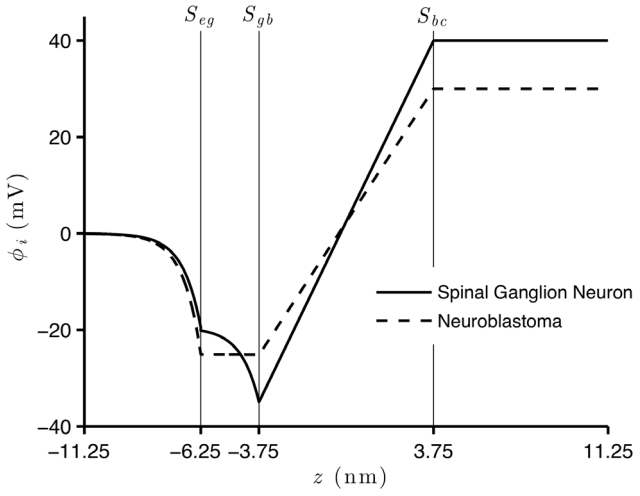

Figure 5. Electric potential across the membranes of spinal ganglion neurons and neuroblastoma cells, during AP state. Solutions of Eq. (52) with boundary $\phi_{S_{eg}}$, and Eq. (45) with boundary $\phi_{+\infty}=\phi_A$ result respectively in $\phi_{S_{gb}}=-34.97$ mV and $\phi_{S_{bc}}=39.99$ mV, for the spinal ganglion neuron (solid), and for the neuroblastoma cell (dashed) in $\phi_{S_{gb}}=-25.17$ mV and $\phi_{S_{bc}}=29.99$ mV. For all simulations, $Q_{S_{bc}}=30Q_{S_{eg}}$ and $\rho_{fc}=20\rho_{fg}$.
doi:10.1371/journal.pone.0096194.g005

by the negative charges spatially distributed in the cytoplasm. Even though the net value of charges of proteins is predominantly negative in the cytoplasm, our simulations indicate that the contribution of these charges to the intracellular potential profile is much smaller than the effect of charges fixed on S_{bc}. This is shown by the curvature of the potential in the cytoplasmic region.

The neuroblastoma cells, like all cancerous cells, multiply quickly. Alterations of the dynamics of cellular multiplication mediate changes in the synthesis, structure and degradation of the membrane components [11], which result in deformations on the structure and composition of the surfaces of membranes [23]. These deformations provoke changes in the composition of electric charges on the membrane. Our results indicate that the alteration of these charges and of those within the cells may influence the behavior of the potential on the inner surface of the neuroblastoma cells.

Experimental observations have suggested that the resting state and the generation of action potentials in human neuroblastoma cells depend on the degree of the morphological differentiation of the cell. Some of these cells are relatively non-excitable [24,25]. Kuramoto et al. [26] stimulated the growth of SK-N-SH human neuroblastoma cells under standard culture conditions. These cancerous cells remained morphologically undifferentiated, partially responded to injections of pulses of electric current, and presented deficiency of the depolarizing component of the mechanism that generates the action potential. We included these findings in our simulations, and Fig. (5) is consistent with the fact that the depolarization of the electric potential in the neuroblastoma, during generation of the action potential, is less intense than in the healthy spinal ganglion neuron. The neuroblastoma should thus generate a lower firing rate in response to its input excitation, and this may affect the transmission of signals through networks of these neurons and their functions of storage and communication of information.

Mironov and Dolgaya [17] have suggested that the outer electric charges for the neuroblastoma cells and erythrocytes are similar, but the spinal ganglion neurons strongly differ from these cells. Therefore, the molecular structure (and the resulting constitution of charges) on the outer surface of the membrane of the neuroblastoma cells would be similar to the erythrocytes, and may be constituted by $\simeq$ 40% of peripheral proteins and $\simeq$ 60% of gangliosides. Our results illustrate that the drop of the potential across the glycocalyx for the neuroblastoma cell is much smaller than for the spinal ganglion neuron, during both resting and AP states. This corroborates previous studies which show a smaller decay of the potential for the erythrocyte in the glycocalyx than for the neuron [2,4,5]. The different behavior of the potential across the glycocalyx, for the neuroblastoma and the spinal ganglion neuron, should indicate important differences among these cells, of the properties that enable the transmission of electric signals through the membrane. This occurs due to the fact that different molecular structures of these membranes interact differently with (i) the outer electric field, which is responsible for the orientation of the charged particles that are closer to the membrane, and (ii) the potential on the outer surface of the membrane. The nature of these interactions are crucial for many cell processes, such as the beginning of the process of triggering of the action potential, which depends on the opening of specific Na^+ channels.

Our results may also contribute to understanding the resistance of the neuroblastoma to certain chemotherapeutic treatments [27,28]. The smaller change of the potential, in response to changes in properties of cellular cultures (pH values, for instance) and to the amount of fixed charges present in the membrane due to alterations in its composition and structure, may be an electric property responsible for the low pharmacological response.

Author Contributions

Conceived and designed the experiments: TMP RSW CMC. Performed the experiments: TMP. Analyzed the data: TMP RSW CMC. Contributed reagents/materials/analysis tools: TMP RSW CMC. Wrote the paper: TMP RSW CMC.

References

1. Iglic A, Brumen M, Svetina S (1997) Determination of the inner surface potential of erythrocyte membrane. Bioelectroch Bioener 43: 97–107.
2. Heinrich R, Gaestel M, Glaser R (1982) The electric potential profile across the erythrocyte membrane. J Theor Biol 96: 211–231.
3. Cortez C, Bisch P (1993) The effect of ionic strength and outer surface charge on the membrane electric potential profile: a simple model for the erythrocyte membrane. Bioelectroch Bioener 32: 305–315.
4. Cortez C, Cruz F, Silva D, Costa L (2008) Inuence of fixed electric charges on potential profile across the squid axon membrane. Physica B 403: 644–652.
5. Cruz F, Vilhena F, Cortez C (2000) Solution of non-linear Poisson-Boltzmann equation for erythrocyte membrane. Braz J Phys 30: 403–409.
6. Bolintineanu D, Sayyed-Ahmad A, Davis H, Kaznessis Y (2009) Poisson-Nernst-Planck models of nonequilibrium ion electrodiffusion through a protegrin transmembrane pore. PLoS Comput Biol 5: e1000277.
7. Zheng Q, Wei G (2011) Poisson-Boltzmann-Nernst-Planck model. J Chem Phys 134: 194101.
8. Belan P, Dolgaya E, Mironov S, Tepikin A (1987) Relation between the surface potential of mouse neuroblastoma clone c1300 cells and the phase of the cell cycle. Neirofiziologiya 19: 130–133.
9. Dolgaya E, Mironov S, Pogorelaya N (1985) Changes in surface charge of mouse neuroblastoma cells during growth and morphological differentiation of the cell population. Neirofiziologiya 17: 168–174.
10. Hernandez M, Kisaalita W, Farmer M (1996) Assessment of murine neuroblastoma (N1E-115) resting membrane potential by confocal microscopy. J Fluoresc 6: 77–82.
11. Dehlinger P, Schimke R (1971) Size distribution of membrane proteins of rat liver and their relative rates of degradation. J Biol Chem 246: 2574–2583.
12. Gouy G (1910) Sur la constitution de la charge électrique à la surface d'un électrolyte. Journal de Physique Théorique et Appliquée 9: 457–467.
13. Chapman D (1913) A contribution to the theory of electrocapillarity. Philos Mag 25: 475–481.
14. Debye P, Huckel E (1923) The theory of electrolytes. I. Lowering of freezing point and related phenomena. Physikalische Zeitschrift 24: 185–206.
15. Verwey E, Overbeek J (1948) Theory of the stability of lyophobic colloids. Amsterdam: Elsevier.
16. Dolgaya E, Mironov S (1984) Investigation of surface properties of rat spinal ganglion neuron by microelectrophoresis. Neirofiziologiya 16: 176–182.
17. Mironov S, Dolgaya E (1985) Surface charge of mammalian neurones as revealed by microelectrophoresis. J Membrane Biol 86: 197–202.
18. Raval P, Allan D (1984) Sickling of sickle erythrocytes does not alter phospholipid asymmetry. Biochem J 223: 555–557.
19. Cook G, Heard D, Seaman G (1960) A sialomucopeptide liberated by trypsin from the human erythrocyte. Nature 188: 1011–1012.
20. Cook G (1968) Glycoproteins in membranes. Biol Rev Camb Philos Soc 43: 363–391.
21. Engelhardt H, Gaub H, Sackmann E (1984) Viscoelastic properties of erythrocyte membranes in high-frequency electric fields. Nature 307: 378–380.
22. Jackle J (2007) The causal theory of the resting potential of cells. J Theor Biol 249: 445–463.
23. Schubert D, Humphreys S, de Vitry F, Jacob F (1971) Induced differentiation of a neuroblastoma. Dev Biol 25: 514–546.
24. Gèrard V, Rouzaire-Dubois B, Dilda P, Dubois J (1998) Alterations of ionic membrane permeabilities in multidrug-resistant neuroblastoma x glioma hybrid cells. J Exp Biol 201: 21–31.
25. Kuramoto T, Werrbach-Perez K, Perez-Polo J, Haber B (1981) Membrane properties of a human neuroblastoma II: Effects of differentiation. J Neurosci Res 6: 441–449.
26. Kuramoto T, Perez-Polo J, Haber B (1977) Membrane properties of a human neuroblastoma. Neurosci Lett 4: 151–159.
27. Lindskog M, Spenger C, Jarvet J, Graslund A, Kogner P (2004) Predicting resistance or response to chemotherapy by proton magnetic resonance spectroscopy in neuroblastoma. J Natl Cancer Inst 96: 1457–1466.
28. Michaelis M, Cinatl J, Vogel J, Pouckova P, Driever P, et al. (2001) Treatment of drug-resistant human neuroblastoma cells with cyclodextrin inclusion complexes of aphidicolin. Anticancer Drugs 12: 467–473.
29. Clay J, Shrier A (2001) Action potentials occur spontaneously in squid giant axons with moderately alkaline intracellular pH. Biol Bull 201: 186.
30. Inoue H (2002) Transport of 125I and 36Cl across an anion-exchange paper membrane. Appl Radiat Isot 56: 659–665.
31. Rosenheck K (1998) Evaluation of the electrostatic field strength at the site of exocytosis in adrenal chromaffin cells. Biophys J 75: 1237.
32. Walker J, Halliday D, Resnick R (2011) Fundamentals of Physics. NJ: Wiley: Hoboken, sixth edition.
33. Becchetti A, Arcangeli A, Del Bene M, Olivotto M, Wanke E (1992) Intra and extracellular surface charges near Ca2+ channels in neurons and neuroblastoma cells. Biophys J 63: 954–965.
34. Rosenthal J, Bezanilla F (2002) A comparison of propagated action potentials from tropical and temperate squid axons: different durations and conduction velocities correlate with ionic conductance levels. J Exp Biol 205: 1819–1830.
35. Guyton A, Hall J (1997) Human physiology and mechanisms of disease. Philadelphia: W.B. Saunders Co., sixth edition.
36. Tosetti P, Taglietti V, Toselli M (1999) Action-potential-like depolarizations relieve opioid inhibition of N-type Ca2+ channels in NG108-15 cells. Pug Arch Eur J Phy 437: 441–448.